Full Stokes observations in the He I 1083 nm spectral region covering an M3.2 flare

Christoph Kuckein[1], Manuel Collados[2,3], Rafael Manso Sainz[2,3] and Andrés Asensio Ramos[2,3]

[1]Leibniz-Institut für Astrophysik Potsdam (AIP), D-14482 Potsdam, Germany
email: `ckuckein@aip.de`

[2]Instituto de Astrofísica de Canarias (IAC), E-38205 La Laguna, Tenerife, Spain

[3]Departamento de Astrofísica, Universidad de La Laguna, E-38206 La Laguna, Tenerife, Spain

Abstract. We present an exceptional data set acquired with the Vacuum Tower Telescope (Tenerife, Spain) covering the pre-flare, flare, and post-flare stages of an M3.2 flare. The full Stokes spectropolarimetric observations were recorded with the Tenerife Infrared Polarimeter in the He I 1083.0 nm spectral region. The object under study was active region NOAA 11748 on 2013 May 17. During the flare the chomospheric He I 1083.0 nm intensity goes strongly into emission. However, the nearby photospheric Si I 1082.7 nm spectral line profile only gets shallower and stays in absorption. Linear polarization (Stokes Q and U) is detected in all lines of the He I triplet during the flare. Moreover, the circular polarization (Stokes V) is dominant during the flare, being the blue component of the He I triplet much stronger than the red component, and both are stronger than the Si I Stokes V profile. The Si I inversions reveal enormous changes of the photospheric magnetic field during the flare. Before the flare magnetic field concentrations of up to ~ 1500 G are inferred. During the flare the magnetic field strength globally decreases and in some cases it is even absent. After the flare the magnetic field recovers its strength and initial configuration.

Keywords. Sun: flares, Sun: photosphere, Sun: chromosphere, Sun: magnetic fields, techniques: polarimetric

1. Introduction

Solar flares are among the most dynamic and energetic events observed in the atmosphere of the Sun. The He I 1083.0 nm spectral region offers a unique diagnostic tool to study simultaneously chromospheric and photospheric magnetic fields. Intensity observations in the He I 1083.0 nm triplet have been used in the past to study flares at the limb (e.g., You & Oertel 1992), and on the disk (e.g., Malanushenko 1999; Du & Li 2008; Li *et al.* 2007), and the formation of the intensity profile theoretically considered (e.g., Ding *et al.* 2005). Circular polarization measurements in flares have been carried out by Penn & Kuhn (1995). More recently, several works using the He I triplet in flares have appeared. Zeng *et al.* (2014) have presented high resolution filtergrams of a C-class flare to study the mechanism which leads to He I 1083.0 nm emission. Akimov *et al.* (2014) have described an X1.4 flare as observed with a spectroheliograph in the vicinity of He I 1083.0 nm. Using spectropolarimetry Sasso *et al.* (2011, 2014) have covered a C2.0 flare with one spectral scan and focused their analysis on the magnetic structure of an activated filament. Finally, Judge *et al.* (2014) have presented observations that cover the evolution of an X1.0 flare. These authors concentrate on several aspects of the flare, among others, the photospheric magnetic field before and after the flare.
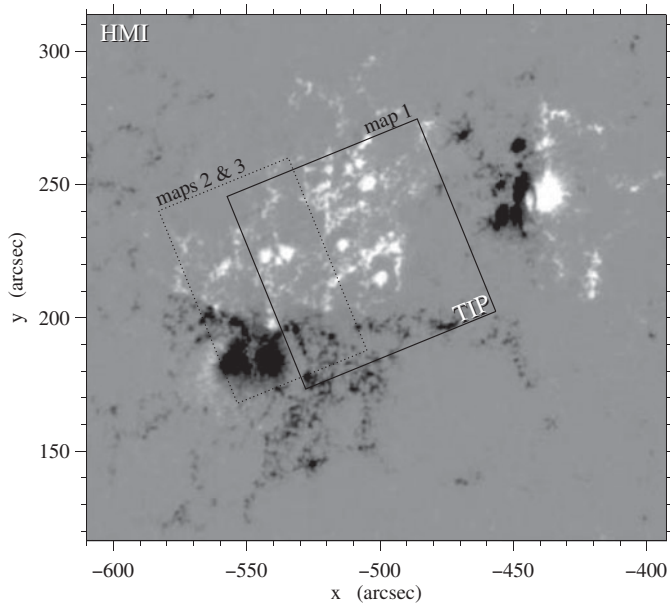
Figure 1. HMI line of sight (LOS) magnetogram of active region NOAA 11748 on 2013 May 17 at 08:57 UT. The magnetogram is clipped between ± 700 G. A filament was lying on top of the PIL. The solid and dashed boxes show the approximate scanned area of TIP-II. Solar north and west correspond to up and right.

The full Stokes observations in the He I 1083.0 nm spectral region presented in this work cover the pre-flare, flare, and post-flare stages of an M3.2 flare. Fortunately, the slit was at the right time and position, covering the whole evolution of the flare. The first results concerning the evolution of the photospheric magnetic field have been recently published by Kuckein *et al.* (2015).

2. Observations

Active region NOAA 11748 produced 14 flares, between classes C and X. On 2013 May 17, an M3.2 flare was captured with the telescope. The flare started at 8:43 UT and finished at 9:19 UT. The peak of the flare occurred at 8:57 UT. The ground-based observations were carried out with the Tenerife Infrared Polarimeter (TIP-II; Collados *et al.* 2007) attached to the Echelle spectrograph of the Vacuum Tower Telescope (VTT; Tenerife, von der Lühe 1998). The main target was a filament lying on top of the polarity inversion line (PIL) at coordinates (N 11°, E 36°). The first scan with the slit, from 7:48 to 8:36 UT, was the largest scan and covered 77″ in the scan direction. This map covered the pre-flare stage. The second map, from 8:36 to 9:06 UT, was smaller and covered 52.5″ in the scan direction. In this map the slit passed over the flare at its peak ($\sim$ 8:57 UT). The third map, from 9:06 to 9:37 UT, covered the same spatial area as the previous map and included the post-flare phase of the flare. All three scanned regions are superimposed in Fig. 1 on a context magnetogram of the Helioseismic and Magnetic Imager (HMI; Schou *et al.* 2012) on board the Solar Dynamics Observatory (SDO; Pesnell *et al.* 2012).

The spectral range included full Stokes spectropolarimetry in the He I 1083.0 nm vicinity. The spectra contained the photospheric Si I line at 1082.7 nm, the chromospheric He I triplet, which comprises three spectral lines (the "blue" component at 1082.9 nm and the

blended "red" component at 1083.0 nm), and two telluric lines. The spectral sampling was ~ 11.1 mÅ/pixel. The exposure time per slit position was 10 s and the scanning step $0.35''$. The pixel size along the slit was $0.17''$. The Kiepenheuer-Institute Adaptive Optics System (KAOS; Berkefeld *et al.* 2010) was locked on small structures, like pores and small penumbrae, and significantly improved the image quality under fair seeing conditions.

Flare processes are complex phenomena which involve many different layers of the solar atmosphere. In this study, we simultaneously compare two different layers. The formation height of the He I triplet corresponds to the upper chromosphere (Avrett *et al.* 1994) while the photosphere is represented by the Si I line (e.g., Bard & Carlsson 2008).

3. Data reduction

All data sets were corrected for flat-field and dark frames. Moreover, the standard polarimetric calibration for the TIP-II instrument was carried out (Collados 1999, 2003).

For the normalization procedure of the Stokes profiles we computed a continuum value for each position of the slit. This was needed because the intensity level changed throughout the scans because of changing air mass and center-to-limb variations. For this purpose we used all available maps from that day (six maps). In each map, several scans were averaged along the slit over a quiet Sun area. Afterwards, a second-order least-square polynomial fit was carried out to retrieve the quiet Sun continuum values individually for each scan step. All pixels along the slit within one scan step were divided by their corresponding quiet Sun continuum value.

The wavelength calibration was carried out using the two nearby-lying telluric lines. In an averaged quiet Sun area, we calculated the distance between both telluric lines and compared it with the distance separating the same telluric lines in the Fourier Transform Spectrometer spectrum (FTS; Neckel & Labs 1984). The division of both distances yielded the spectral sampling. We followed the procedure explained in Appendices A and B of Kuckein *et al.* (2012) to retrieve the wavelength axis on an absolute scale, i.e., corrected for Earth's orbital motions, solar rotation, and the solar gravitational redshift.

4. Results and discussion

4.1. *Analysis of the Stokes profiles*

The data sets in Fig. 2 are represented as monochromatic slit-reconstructed intensity images. The upper row shows the line core of the He I red component and the time range of the scans. The three panels correspond to the pre-flare, flare, and post-flare scans, respectively. In the first scan, we focus on the image inside the dashed box, which outlines the common part of the FOV between all three maps. A filament is lying on top of the PIL. In addition, two pores are seen above the filament at around $y \sim 53''$. The middle panel shows the flare phase. Strong He I 1083.0 nm emission can be identified between the filament and the pores. Turning to the third panel, which is aligned with the middle panel, the presence of post-flare loops is clear. These loops must have formed very quickly (< 30 min). There is still some emission of He I in the post-flare map, but weaker (see the colorbar) and in a different area of the FOV.

The lower three panels in Fig. 2 show the pre-flare, flare, and post-flare maps as seen in the normalized Si I line core intensity. Although the line core gets shallower during the flare (see the colorbar in the middle panel), by far it never goes into emission.
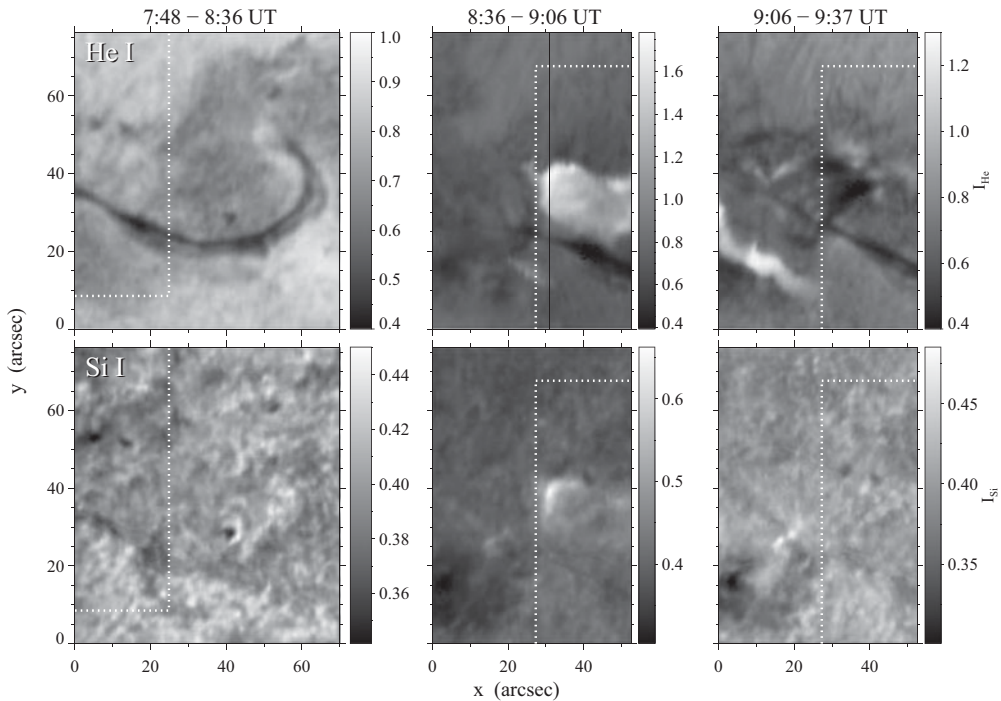
Figure 2. Monochromatic slit-reconstructed images of the red component of He I (upper row) and the Si I line core (lower row). The different stages of the flare are shown from left to right: pre-flare, flare and post-flare maps. The dashed boxes indicate the common area between all three maps. The overlapping area can also be identified in Fig. 1. The vertical solid line in the middle map shows the location of the Stokes profiles in Fig. 3.

Examples of Stokes profiles during the flare are shown in Fig. 3. Starting in the upper left corner and counting clockwise: Stokes I, Q, V, and U. Note that the normalized Stokes parameters are given on different scales for each panel. The profiles correspond to the vertical solid line shown in the upper middle panel of Fig. 2. The Stokes I panel shows a broad vertical line on the lefthand which corresponds to the Si I line. The next two lines to the right correspond to the He I triplet. The single most striking observation from this panel is the strong emission of the He I triplet, with an intensity ratio to the continuum of up to ~ 1.86. Some emission profiles seem to be strongly redshifted as they almost reach the second telluric line. Similarly, redshifts occur in the absorption profiles which correspond to the filament at $y \sim 24''$.

The linear polarization, Stokes Q and U panels, are clipped between ± 0.005. Especially in the area were the flare occurs (He I emission, $I > 1$), one-lobe polarization signatures are found that cannot be ascribed to the typical Zeeman shapes. Interestingly, both the blue and red components of the He I triplet show linear polarization signatures of the same sign. As for the Stokes V panel (saturated at ± 0.02), there is significant circular polarization seen in the He I triplet during the flare. Curiously, the He I Stokes V profile is reversed with respect to the Si I one where the flare occurs. This happens because only He I goes into emission during the flare. Additionally, during the flare the Stokes V amplitude is larger in He I as compared to Si I. Furthermore, the He I Stokes V amplitude of the blue component is significantly larger than the Stokes V amplitude of the red component. The profile of the red lobe of Stokes V from the red component of He I is
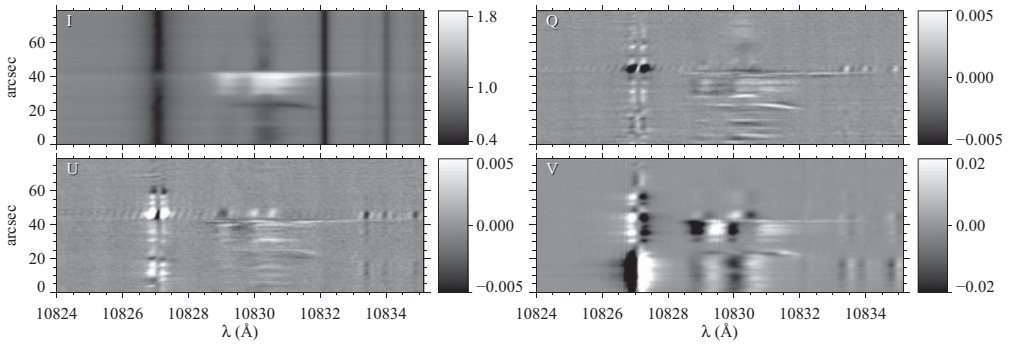
Figure 3. Starting top left and moving clockwise: normalized Stokes profiles I, Q, V, and U. The profiles correspond to the vertical solid line in the top-middle panel in Fig. 2. From left to right the following spectral lines can be seen: Si I, the He I triplet, and two telluric lines. Stokes Q and U are clipped at ± 0.005 and Stokes V at ± 0.02.

broad and somehow displaced and stretched towards bigger wavelengths (redshifted). This is not the case for the blue component nor for the Si I Stokes V profiles.

4.2. *Photospheric magnetic field*

We carried out full Stokes inversions of the photospheric Si I line using *Stokes Inversions based on Response functions* (SIR; Ruiz Cobo & del Toro Iniesta 1992). The model atmosphere covered a range of the logarithm of the LOS continuum optical depth at 500 nm between $1.4 \leqslant \log \tau \leqslant -4.0$. To infer the magnetic field at the height of granulation, we will focus on a constant height at $\log \tau = -1$. Furthermore, we will concentrate on a region of interest within the FOV which only includes the flare. The region of interest fulfills the criterion that He I goes into emission ($I > 1$, see top-middle panel of Fig. 2). In other words, the region of interest is inside the rectangle with coordinates $x \sim [30'', 50'']$ and $y \sim [25'', 40'']$ in the middle panel of Fig. 2. The same area was analyzed in the pre-flare and post-flare maps. After carefully comparing the inferred photospheric magnetic field before, during, and after the flare we found the following: (1) Concentrations of several seconds of arc of strong magnetic fields (< 1500 G) are seen before the flare. (2) During the flare, the field strength globally decreased and even vanished in some areas. (3) After the flare, the magnetic field has partially recovered its strength and pattern. Kuckein *et al.* (2015) presented a detailed map of the photospheric magnetic field and the associated Doppler velocities.

We conclude that remarkable changes of the photospheric magnetic field of up to 1500 G are found during this M3.2 flare. These changes happen in short time periods ($\leqslant 30$ min). While changes of the photospheric magnetic field during flares have been reported in the past (e.g., Petrie & Sudol 2010), such a strong decrease was not seen before.

A natural progression of this work is to invert the He I triplet and infer the chromospheric magnetic field and Doppler velocities. In terms of directions for future research, further multi-height and multi-wavelength observations of the evolution of flares are crucial. A promising telescope for carrying out such observations is the 1.5-meter GRE-GOR telescope (Schmidt *et al.* 2012) located at the Observatorio del Teide in Tenerife. The combination of its two principal instruments, the GREGOR Infrared Spectrograph (GRIS; Collados *et al.* 2012) equipped with TIP-II and the GREGOR Fabry-Pérot Interferometer (GFPI; Puschmann *et al.* 2012) will simultaneously cover several heights in the solar atmosphere. Integrating sensitive near-infrared polarimetry with high spatial and

temporal resolution observations exploits the synergy between scanning spectrographs and imaging spectropolarimeters for flare research.

Acknowledgements

References

Akimov, L. A., Belkina, I. L., & Marchenko, G. P. 2014, *MNRAS* 439, 193

Avrett, E. H., Fontenla, J. M., & Loeser, R. 1994, in: D.M. Rabin, J.T. Jefferies, & C. Lindsey (eds.), *Infrared Solar Physics*, IAU Symp. No. 154 (Dordrecht: Kluwer), p. 35

Bard, S. & Carlsson, M. 2008, *ApJ* 682, 1376

Berkefeld, T., Soltau, D., Schmidt, D., & von der Lühe, O. 2010, *Applied Optics* 49, G155

Collados, M. 1999, in: B. Schmieder, A. Hofmann, & J. Staude (eds.), *Third Advances in Solar Physics Euroconference: Magnetic Fields and Oscillations*, ASP Conf. Series 184 (San Francisco: ASP), p. 3

Collados, M. V. 2003, in: S. Fineschi (ed.), *Polarimetry in Astronomy*, Proc. SPIE 4843, p. 55

Collados, M., Lagg, A., Díaz Garcí, A. J. J., Hernández Suárez, E., López López, R., Páez Mañá, E., & Solanki, S. K. 2007, in: P. Heinzel, I. Dorotovič, & R.J. Rutten (eds.), *The Physics of Chromospheric Plasmas*, ASP Conf. Series 368 (San Francisco: ASP), p. 611

Collados, M., López, R., Páez, E., *et al.* 2012, *AN* 333, 872

Ding, M. D., Li, H., & Fang, C. 2005, *A&A* 432, 699

Du, Q.-S. & Li, H. 2008, *Chinese J. Astron. Astrophys.* 8, 723

Judge, P. G., Kleint, L., Donea, A., Sainz Dalda, A., & Fletcher, L. 2014, *ApJ* 796, 85

Kuckein, C., Martínez Pillet, V., & Centeno, R. 2012, *A&A* 542, A112

Kuckein, C., Collados, M., & Manso Sainz, R. 2015, *ApJ* (Letters) 799, L25

Li, H., You, J., Yu, X., & Du, Q. 2007, *Solar Phys.* 241, 301

Malanushenko, E. V. 1999, *Astronomical and Astrophysical Transactions* 18, 273

Neckel, H. & Labs, D. 1984, *Solar Phys.* 90, 205

Penn, M. J. & Kuhn, J. R. 1995, *ApJ* (Letters) 441, L51

Pesnell, W. D., Thompson, B. J., & Chamberlin, P. C. 2012, *Solar Phys.* 275, 3

Petrie, G. J. D. & Sudol, J. J. 2010, *ApJ* 724, 1218

Puschmann, K. G., Denker, C., Kneer, F., *et al.* 2012, *AN* 333, 880

Ruiz Cobo, B. & del Toro Iniesta, J. C 1992, *ApJ* 398, 375

Sasso, C., Lagg, A., & Solanki, S. K. 2011, *A&A* 526, 42

Sasso, C., Lagg, A., & Solanki, S. K. 2014, *A&A* 561, A98

Schmidt, W., von der Lühe, O., Volkmer, R., *et al.* 2012, *AN* 333, 796

Schou, J., Scherrer, P. H., Bush, R. I., *et al.* 2012, *Solar Phys.* 275, 229

von der Lühe, O. 1998, *New Astron. Revs* 42, 493

You, J. Q. & Oertel, G. K. 1992, *ApJ* (Letters) 389, L33

Zeng, Z., Qiu, J., Cao, W., & Judge, P. G. 2014, *ApJ* 793, 87